Journal of Energy Storage 96 (2024) 112693

Contents lists available at ScienceDirect

Journal of Energy Storage

journal homepage: www.elsevier.com/locate/est

Research papers

Mitigating PTFE decomposition in ultra thick dry-processed anodes for high energy density lithium-ion batteries

Seungmin Han [a,b,1], Eui-Hyurk Noh [c,d,1], Sujong Chae [e,1], Kihwan Kwon [a,g], Juhyun Lee [a,f], Ji-Su Woo [c], Seongsu Park [e], Jung Woo Lee [f], Patrick Joohyun Kim [g], Taeseup Song [b,*], Won-Jin Kwak [c,*], Junghyun Choi [a,h,**]

[a] Energy Storage Materials Center, Korea Institute of Ceramic Engineering and Technology, Jinju 52851, Republic of Korea
[b] Department of Energy Engineering, Hanyang University, 222 Wangsimni-ro, Seongdong-gu, Seoul 04763, Republic of Korea
[c] School of Energy and Chemical Engineering, UNIST, Ulsan 44919, Republic of Korea
[d] Department of Energy Systems Research, Ajou University, Suwon 16499, Republic of Korea
[e] Department of Industrial Chemistry, Pukyong National University, 45 Yongso-ro, Nam-gu, Busan 48513, Republic of Korea
[f] Department of Materials Science and Engineering, Pusan National University, Busan 46241, Republic of Korea
[g] Department of Applied Chemistry, Kyungpook National University, Daegu 41566, Republic of Korea
[h] School of Chemical, Biological and Battery Engineering, Gachon University, Seongnam-si, Gyeonggi-do 13120, Republic of Korea

ARTICLE INFO

Keywords:
Lithium-ion batteries
Dry-processed anode
Thick film electrode
Fluoroethylene carbonate
Electrolyte additive

ABSTRACT

Dry electrode technology is a next-generation method for manufacturing lithium-ion batteries because it is useful for fabricating thick electrodes without solvents, facilitating high energy densities and cutting down on the battery manufacturing costs. However, the commonly used polytetrafluoroethylene (PTFE) binder in dry electrode technology undergoes severe decomposition in dry-processed anodes during the first lithiation process due to its low lowest unoccupied molecular orbital level. This phenomenon seriously aggravates battery performance, such as in terms of the initial coulombic efficiency and cycle life. Thus, a strategy to suppress this irreversible reaction of PTFE should be established for dry-processed anodes to increase the energy density of LIBs without adverse effects on battery performance. To address this challenge, in this work, fluoroethylene carbonate (FEC) as an electrolyte additive has been introduced to form a preemptive and stable FEC-derived solid electrolyte interface (SEI) to protect a graphite and the PTFE binder. This SEI considerably alleviates the irreversible reaction of PTFE, thereby securing the reversible capacity and maintaining the structure of the electrode through the great binding properties. These results provide guidance for increasing the electrochemical stability in dry-processed anode systems, which gets closer the innovative dry anode technology for cost-effectiveness and high energy density.

1. Introduction

With the importance of carbon neutrality being raised around the world, electric vehicles (EVs) are gaining considerable attention as substitutes for gasoline-powered vehicles in the transportation sector [1–3]. Lithium-ion batteries (LIBs) are being considered energy storage devices to replace internal combustion engines, due to the decrease in carbon emission by eliminating the use of fossil fuels and the potential of high energy density compared with other battery systems [4–7]. However, conventional LIBs have lower energy density than internal combustion engines, affecting various factors, such as driving range, charge capacity, fast charging, weight, and cost [8,9]. Therefore, it is crucial to improve the energy of LIBs to make them a practical replacement for internal combustion engines.

Recently, dry electrode technology has been gaining remarkable attention for achieving high energy density and high mass loading while reducing manufacturing costs and the carbon emissions from the manufacturing process [10–12]. The conventional electrode

* Corresponding authors.
** Correspondence to: J. Choi, School of Chemical, Biological and Battery Engineering, Gachon University, Seongnam-si, Gyeonggi-do 13120, Republic of Korea.
E-mail addresses: tssong@hanyang.ac.kr (T. Song), wjkwak@unist.ac.kr (W.-J. Kwak), junghchoi@gachon.ac.kr (J. Choi).
[1] These authors contributed equally to this work.

https://doi.org/10.1016/j.est.2024.112693
Received 20 December 2023; Received in revised form 21 May 2024; Accepted 16 June 2024
Available online 24 June 2024

manufacturing technology is based on a wet process including the slurry preparation comprising of electrode materials and solvent, the slurry coating, and drying [10,13]. Wet electrode technology typically uses N-Methyl-2-Pyrrolidone (NMP) as a solvent, which incurs carbon dioxide (CO_2) emissions and leads to increased manufacturing costs due to high-temperature drying and solvent recovery processes [13–15]. Although the solvent replacement from NMP to water in the anode would be a great advantage for the environment, there still are several drawbacks to a drying stage. In the fabrication of a thick electrode through the wet process, the evaporation of solvent during drying high mass-loaded slurry can disarrange the binder distribution over the electrode by migration of binder and even arouse the internal crack in the electrode [16,17]. Furthermore, the clogging of the electrode surface caused by the migrated binder interrupts electrolyte permeability and lithium (Li) ion diffusivity [18]. By contrast, dry electrode technology without utilizing solvent for slurry preparation eliminates the drying process for solvent evaporation, which provides distinct advantages in both carbon emissions and processing costs [10,19]. Moreover, the fabrication of thick electrodes via dry electrode technology enables the preservation of the compositional homogeneity throughout the electrode [20]. This simple yet significant change in the electrode manufacturing process, achieved by eliminating solvents, leads to the easy production of high mass-loaded electrode with high energy density, shortens the manufacturing process, and promotes environmental sustainability [21].

Typically, dry electrode technology makes use of a polytetrafluoroethylene (PTFE) polymer as a binder instead of the conventional polyvinylidene (PVDF) fluoride or sodium carboxymethyl cellulose–styrene butadiene rubber (CMC-SBR), forming a fibrous structure to provide support for active materials [22–24]. This PTFE binder undergoes fibrilization through shear mixing and calendering with other electrode materials [25–27], thus enhancing its binding properties through high specific areas [10]. For manufacturing cathode electrode, the dry electrode technology using PTFE has demonstrated enhancing the energy density and cost-effectiveness [19,28]. Shirley Meng's group fabricated a high-loading $LiNi_{0.5}Mn_{1.5}O_4$ (LNMO) cathode via dry electrode technology using a PTFE binder [19]. Compared with a wet electrode cathode, the dry-processed cathode exhibited high mechanical properties and low polarization, which stabilized its electrochemical performance. However, when it comes to the use of PTFE as a binder for anode, it is acknowledged that PTFE is electrochemically unstable during the lithiation process due to its low lowest unoccupied molecular orbital (LUMO) [22,29–31]. During initial lithiation process, PTFE undergoes defluorination due to its facile electron acceptability, a reaction that can be represented as follows:

$$-(CF_2-CF_2)_n + 4n\,Li^+ \Rightarrow -(C\equiv C)_n + 4n\,LiF \quad (1)$$

This equation reported by Soshi et al. clearly illustrates the formation of lithium fluoride (LiF) and amorphous carbon [32]. This irreversible decomposition not only lowers the initial Coulombic efficiency (ICE) but also reduces the binding properties of PTFE, which significantly deteriorates long-term electrochemical cell performance [22,33]. Therefore, an efficient solution for mitigating the instability of PTFE binder in anodes should be developed to enable the adoption of dry electrode technology for both anode and cathode electrodes (Fig. 1).

In this study, we assessed fluoroethylene carbonate (FEC) as an electrolyte additive to explore how FEC-derived solid electrolyte interphase (SEI) affects the irreversibility of PTFE binders and the electrochemical stability in dry-processed anode. The FEC-derived SEI diminished the irreversible side reactions of the PTFE binder, leading to improving the ICE. The SEI also maintained the structural integrity of the PTFE binder. The alleviated PTFE degradation suppressed volume changes during cycling, resulting in the long-term cycle stability of the electrode. This approach provides the potential to address challenges related to the practical application of dry-processed anodes caused by the irreversible reaction of PTFE. Notably, this is the first report focusing on alleviating PTFE decomposition in dry-processed anodes using FEC, establishing a clear path for enhancing cyclability compared to systems without FEC. Additionally, we established full cell with a high areal capacity using dry-processed anode and cathode electrodes for the first time. Due to the synergistic effects of the FEC-derived SEI, the dry-processed electrode design achieved high cycle stability and high-rate performance.

2. Experimental section

2.1. Electrode fabrication

Graphite, carbon black, and PTFE were prepared as the active material, conductive agent, and binder, respectively, to fabricate a dry-processed anode. The mass ratio of graphite, carbon black, and PTFE was 96:1:3. The fabrication steps were as follows. Premixing was performed using a planetary mixer (ARE-310, Thinky) with a 5 mm zirconia ball and a vortex mixer (VM-10, WiseMix) to prevent the agglomeration of the solid components, such as graphite and carbon black, and the PTFE binder. Then, the well-dispersed mixture powders were shear-mixed using a mortar and pestle for a fabrication of sheet. However, the kneaded sheet was not subjected to enough force for a uniformly fibrillated electrode. To solve this problem, we bent it in half and repeat the calendered by utilizing roll-to-roll calender machine. This thoroughly fiberized film was calendered with a target mass loading of 14.4

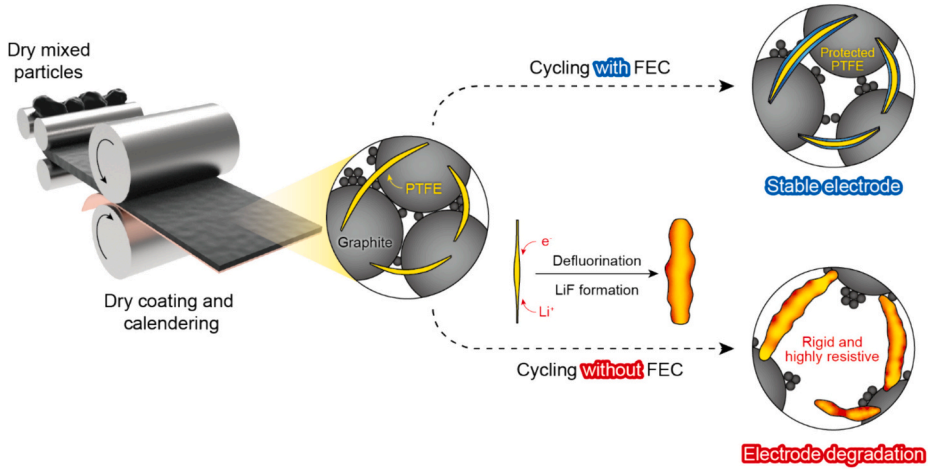

Fig. 1. Schematic illustration of PTFE degradation in dry-processed anode without and with FEC.

mg cm^{-2} (areal capacity: 4.8 mAh cm^{-2}), subsequently laminated onto pretreated copper (Cu) current collector. After calendering, thickness and electrode density of this dry-processed anode without Cu current collector was about 92 μm and 1.55 g cm^{-3}, respectively. This fabricated dry-processed anode was examined via cross-sectional scanning electron microscopy (SEM) image and energy-dispersive X-ray spectroscopy (EDS) mapping (Fig. S1). The homogeneous distributions of C and F in the dry-processed anode were visible via EDS mapping, demonstrating that PTFE is well fibered between the graphite particles. Moreover, the laminated Cu foil was displayed without peeling from dry-processed anode. These series of process proved that the dry-processed anode was successfully fabricated. In addition, The LFP (LFP-NCO, Advanced Lithium Electrochemistry Co. Ltd) with reversible discharge capacity of 162 mAh g^{-1} electrodes were fabricated for the full cell. The mass ratio of LFP:carbon black:binder was 94:3:3 in both high and ultra-high mass loading level LFP electrodes. The thickness of LFP electrodes with high and ultra-high mass loading level were around 185 and 350 μm, respectively.

2.2. Cell assembly

In a dry room where the dew point was kept below −60 °C, the coin cells (2032 R type) were assembled to evaluate their electrochemical performances. For the assembly of half cells, 1.0 T Li metals with a 16 mm diameter were utilized as the counter electrode. For the full cells, the dry-processed anode was coupled with an LFP as a cathode where N/P ratio was 1.1. In both cases, the commercial polyethylene (PE) separators with thickness of 16 μm and diameter of 19 mm, a 1.0 T spacer and two electrolytes were used. The two electrolytes were as follows: 1) 1.15 M lithium hexafluorophosphate ($LiPF_6$) in a mixture of ethylene carbonate (EC), ethyl methyl carbonate (EMC), and diethyl carbonate (DEC) (2:4:4 vol%) containing 1 wt% vinylene carbonate (VC) and 2) 1.15 M $LiPF_6$ in an EC–EMC–DEC mixture (2:4:4 vol%) containing 1 wt% VC and 10 wt% fluoroethylene carbonate (FEC). These pre-mixed electrolytes were purchased from enchem and added to both half and full cells in 200 μL volumes using micro pipette.

2.3. Electrochemical measurements

To verify the redox peak in each different electrolyte, the cyclic voltammetry (CV) analysis was performed at a constant scan rate of 0.1 mV s^{-1} in the range of 0.05–1.5 V using a potentiostat (WBSCS 3000Ls, WonATech). In the case of the halfcells, the galvanostatic charge–discharge cycle test was conducted at 0.3C within the working window of 0.05 V to 1.5 V. For the full cells, after the formation step, the cycle tests were proceeded at 0.2C with the constant voltage mode from 2.5 V to 4.0 V. After the 1 cycle as formation step at 0.1C, the rate capability tests were performed at a fixed charging rate of 0.2C within various discharging rates at 0.1, 0.2, 0.3, 0.5, 1.0, and 1.5C. The electrochemical impedance spectroscopy (EIS, VSP, Biologic, Seyssinet-Pariset) was recorded in the frequency range of 250 kHz–10 mHz to investigate the resistances of the cells. For EIS analysis, Li||Li symmetric cells were evaluated for only one cycle at current density of 0.48 mA cm^{-2} for 10 h in each plating/stripping step under the same operating conditions of the half cells.

2.4. Characterization

Unlike the electrodes before cycle test, the dry-processed anodes with and without FEC were separated from the disassembled cells after the end of the delithiation process and retrieved for postmortem analysis after cycling test. These anodes were rinsed with DEC in an argon-filled glove box to remove the remaining salt on their surfaces. The anode surfaces and cross-sectional morphologies were observed via Field emission SEM (FE-SEM, SU8220, Hitachi). All samples for cross-sectional imaging were processed using a cross-sectional polisher (IB-09020CP, JEOL). The EDS instrument (Ultim Extreme, Oxford) attached to the FE-SEM device as an accessory was used to detect the elements of dry-processed anodes. The X-ray Photoelectron Spectroscope (XPS) analysis was conducted to investigate the composition and chemical bonding of the electrode surfaces. The F 1 s and C 1 s spectra were obtained through XPS. High-Resolution Transmission Electron Microscopy (HRTEM) analysis was introduced to observe the SEI layer of dry-processed anode after 1 cycle. The mechanical properties of the electrodes after 1 cycle were examined via nano indenter (HM2000, FISCHERSCOPE) and surface and interfacial cutting analysis system (SAICAS, SAICAS EN-EX, DAIPLA WINTES). To clarify the decomposition of PTFE in the different electrolytes, the specific analyses was performed using electrodes with an increased composition of PTFE (graphite:carbon black:PTFE binder = 4:1:5). The specific analyses are as follows. X-ray Diffraction (XRD, D8 ADVANCE, BRUKER) spectra was measured to determine the intensity of PTFE peak. The Raman spectra were acquired with Raman microscope (LabRAM Aramis, Horbia Jobin Yvon).

3. Results and discussion

3.1. Electrochemical properties of PTFE binder in dry-processed anode

It is widely acknowledged that PTFE has electrochemical instability in anodes because it readily accepts electrons because of its low LUMO level [26,30]. To identify the unfavorable reductive decomposition of PTFE in a dry-processed graphite anode, the cyclic voltammetry (CV) analysis was carried out at scanning rate of 0.1 mV s^{-1} (Fig. 2a). A strong reduction peak was observed between 0.3 and 0.55 V, which corresponded to the voltage region where PTFE decomposition occurs in previous research [29,30]. The addition of FEC to the electrolyte generated a reduction peak indicating the formation of the FEC-derived SEI layer at approximately 0.9 V (Fig. S2). Additionally, the reduction peak attributed to PTFE decomposition significantly decreased, indicating that the FEC-derived SEI formed prior to PTFE reduction could protect the PTFE from the reduction reaction. This suggests that FEC additive alleviates the decomposition of PTFE, thereby potentially preventing the loss of reversible capacity. Notably, after the second cycle, the CV curves prominently feature peaks indicative of lithium-graphite compound formation, underscoring the improved electrochemical activity in the presence of FEC (Fig. S3). These findings substantiate the crucial role of FEC additive not only in preventing PTFE decomposition but also in promoting a more stable and effective SEI layer formation on graphite surface.

In order to confirm the influence of FEC additive on the battery performance of dry-processed anode, the galvanostatic charge-discharge voltage profiles in the first cycle at 0.05–1.5 V (vs. Li/Li^+) are presented in Fig. 2b. In accordance with the CV analysis findings (Fig. 2a), PTFE decomposition reaction is observed at the first lithiation in dry-processed anode without FEC. This reductive decomposition during lithiation caused a large irreversible capacity (107.6 mAh g^{-1}) and a low initial cycle efficiency (ICE, 75.7 %). On the other hand, the preemptive reduction of FEC suppressed the decomposition of PTFE in the dry-processed anode, as shown in the voltage profile during the lithiation (Fig. 2b). The mitigation of PTFE decomposition by FEC considerably enhanced the ICE to 87.2 % which is 11.5 % higher than that of the sample without FEC (Fig. 2c). Besides, it is notable that the reversible capacity of the dry-processed anode without FEC (335.5 mAh g^{-1}) was smaller than that of the dry-processed anode with FEC (347.4 mAh g^{-1}). As the overall voltage profiles of the two samples at a low C-rate (0.1C) were almost overlapped without overpotential throughout the delithiation process, the decreased capacity from the PTFE decomposition at the first cycle could be ascribed to the loss of active material rather than an increase of in resistance.

Fig. 2d exhibits the cycling performances of the dry-processed graphite anodes with and without FEC at 0.3C (1C = 4.8 mA cm^{-2})

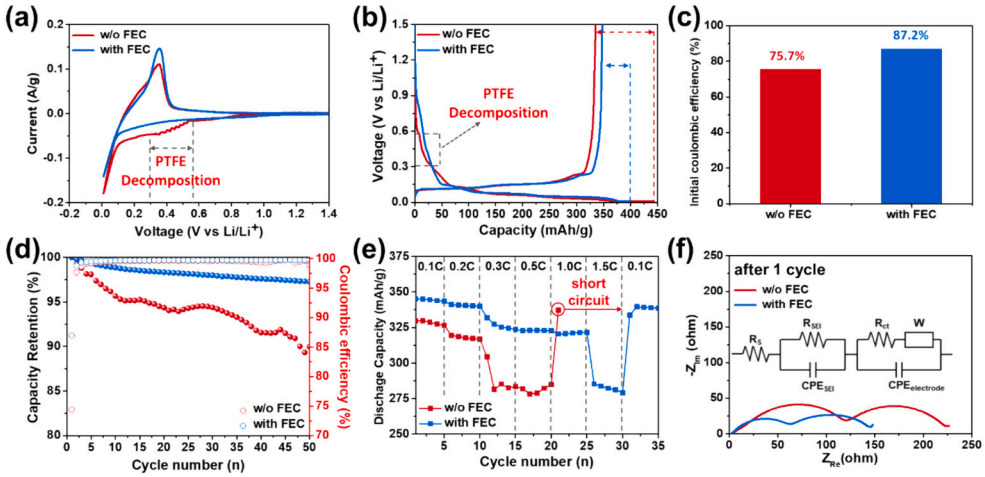

Fig. 2. Electrochemical performances of half cells using dry-processed anodes without and with FEC. (a) CV curves, (b) Voltage profiles after 1 cycle, (c) Initial Coulombic efficiency attributed voltage profiles after 1 cycle, (d) Cycling performances for 50 cycles, (e) Rate capabilities at various C-rates, and (f) Nyquist plots after 1 cycle and inset illustration for the equivalent circuit.

for 50 cycles. The dry-processed anode with the FEC additive demonstrated superior capacity retention (97.3 %) over the anode without FEC (89.9 %) after 50 cycles, as well as stable cycling coulombic efficiencies. The corresponding discharge capacity profiles at 1st, 5th, 10th, 25th, and 50th cycles are shown in Fig. S4 (Supporting Information). These excellent cycle performances with the FEC additive indicates that the graphite and PTFE, protected by FEC at the first cycle, could maintain a binding network in the electrode against the volume change (~10 %) of the graphite during cycling, enabling to exploit the capacity of the whole electrode [34]. Moreover, a rate capability test was performed by varying the discharging rate from 0.1 to 1.5C. The dry-processed anode with FEC showed astonishing rate capabilities at all rates compared with the dry-processed anode without FEC. Contrastingly, the poor rate capability is observed even at 0.3C in the dry-processed anode without FEC, and unstable cycling behavior with an electrical short circuit occurs at 1C (Fig. 2e). Fig. S5 provides the voltage profiles discharge capacities corresponding rate capability test with an increasing C-rate. This degraded rate performance is because the large resistance originated from the severe PTFE decomposition hindered the fast mobility of the Li ions in the interface, which can be supported by the Electrochemical impedance spectroscopy (EIS) results after 1 cycle (Figs. 2f and **S6**). The semicircles in the Nyquist plot of half cells were deconvoluted based on the equivalent circuit in the inset (Fig. 2f). The bulk resistance (R_s), SEI resistance (R_{sei}), charge transfer resistance (R_{ct}), and total resistance values for the dry-processed anode with FEC had lower than those of the electrode without FEC, represented in Table S1. However, Li metal is significant affected by the electrolyte, current, and deformed morphology during cycling due to its low surface area [35–37]. Thus, the additional EIS analysis of Li||Li symmetric cells using electrolyte without and with FEC after 1 cycle was conducted to consider the influence of Li metal in the half cells (Fig. S6). Based on resistance values of Li||Li symmetric cells without and with FEC, the resistance between one side of the Li metal and the electrolyte was deduced to be 76.6 Ω and 60.9 Ω, respectively. By subtracting the resistance of Li metal in electrolyte from the total resistance, the resistance of the electrodes within each electrolyte was calculated, which proves that the resistance of the electrodes with FEC (93.7 Ω) is still lower than without FEC (158.9 Ω). These low resistances are directly related to the alleviated electrode degradation by inhibiting the PTFE decomposition, leading to fast Li-ions migration and facilitation of the charge transfer reaction. Considering the significant enhancements in electrochemical properties, which is clear that the FEC additive is a highly effective solution for mitigating the degradation caused by PTFE side reactions in the dry-processed anode.

3.2. Chemical properties of PTFE depending on electrolyte additive

From XPS analysis, it was verified that the electrochemical irreversible reaction and poor performance of the cells with the thick electrode without FEC in Fig. 2 resulted from the chemical decomposition of PTFE during the first cycle (Fig. 3). Compared to the results of the dry-processed anode before the cycle test (Fig. S7a), the C-F_2 peak, attributed to pristine PTFE, reduced while the peaks for various carbon by-products were formed after cycling test as shown in C 1s spectra (Fig. 3a). The formation of by-products containing rigid C═C bonds can cause PTFE to lose its flexible properties, thereby reducing the ability of PTFE as a binder through fiberization [38]. After cycling test employing electrolyte with FEC, the decrease in the C-F_2 peak was alleviated, and the shoulder peak was noticeably reduced. These results further prove that effect of FEC to mitigate the decomposition of PTFE is the reason for the improved electrochemical performance in Fig. 2. Also, the decomposition of PTFE was clearly supported through decrease in the C-F_2 (688.6 eV) peak in the F 1s spectra (Figs. 3b and S7b). The result that the decrease in C-F_2 due to PTFE decomposition is alleviated in the presence of FEC is also consistent with what was confirmed by the C 1s spectra. Additionally, the P-F peak appeared relatively larger in the presence of FEC in the F 1s spectra, indicating that the presence of FEC in the electrolyte induces the formation of an anion-derived SEI containing PF_6. The anion-derived SEI layer is known to help stabilize anode surfaces [39,40], and it is inferred that this change in the SEI had an effect in alleviating the decomposition of PTFE. To support the XPS results, High-Resolution Transmission Electron Microscopy (HRTEM) was utilized to measure the thickness of the SEI film. Fig. 3(c–d) shows HRTEM images of the SEI layer on electrodes with and without FEC. These images reveal that electrodes without FEC display a noticeably thicker SEI layer, which aligns with the increased decomposition of PTFE detected in the XPS spectra. Conversely, the presence of FEC is associated with a thinner and more stable SEI layer. This visual confirmation of SEI film demonstrates the effect of FEC in enhancing the electrochemical performance by stabilizing the SEI layer and mitigating the decomposition of PTFE.

To further investigate the PTFE decomposition reaction depending on the addition of FEC to the electrolyte, additional analyses were performed on electrodes with an increased composition of PTFE binder. The analysis results of the dry-processed anode before cycle test are provided in Fig. S8. The decrease in the intensity of XRD peak corresponding to the (100) phase of PTFE was alleviated by adding FEC in electrolyte (Fig. 3e). The Raman spectroscopy also shows the decomposition of PTFE during cycling test and the effect of alleviating PTFE

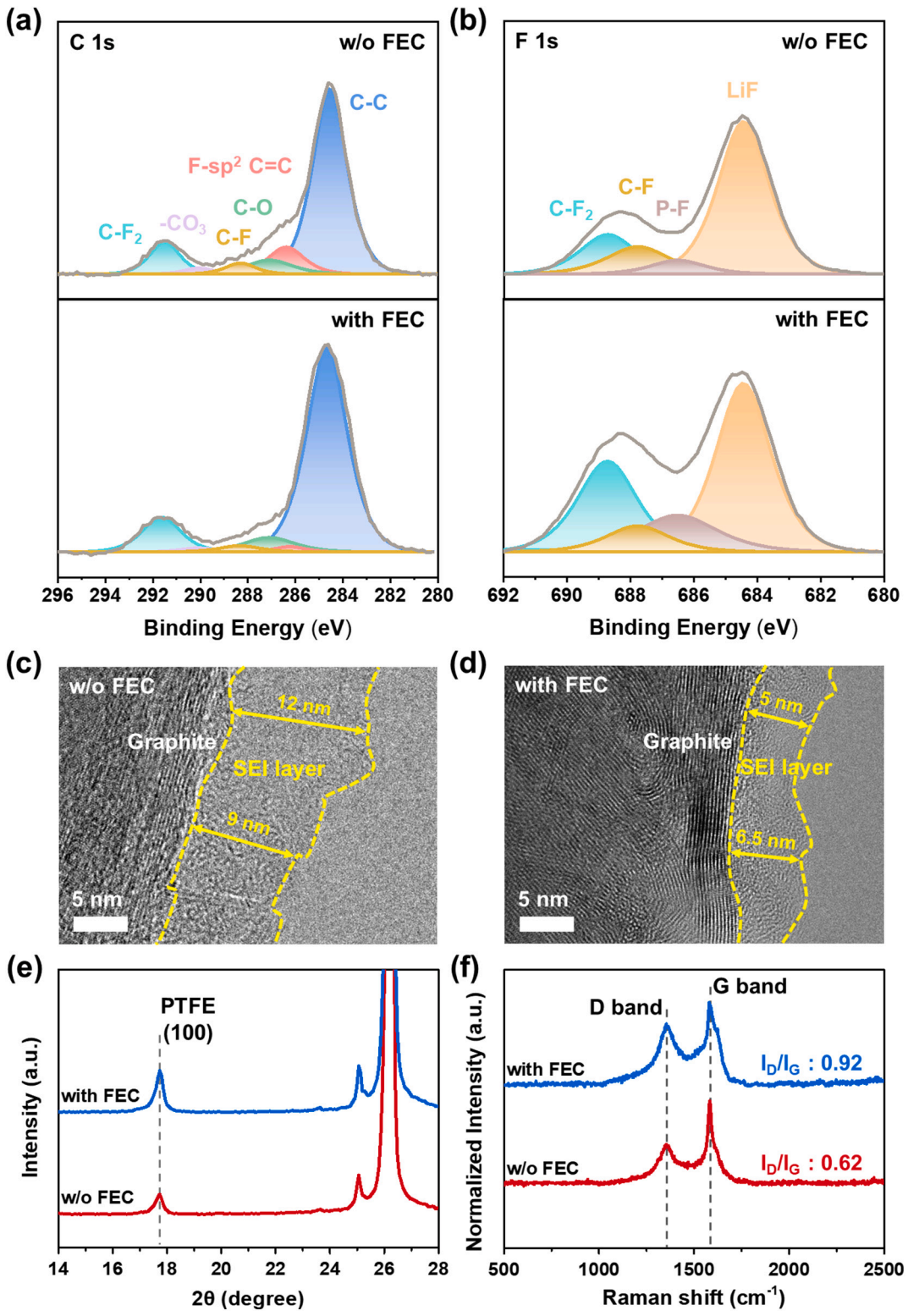

Fig. 3. XPS analysis of dry-processed anode without and with FEC after 1 cycle. (a) C 1s, (b) F 1s spectra; TEM images of dry-processed anode after 1 cycle. (c) without FEC (d) with FEC; The comparison for degree of PTFE decomposition after 1 cycle in dry-processed anode without and with FEC via (e) X-ray diffraction (XRD) and (f) Raman spectra.

decomposition by FEC (Fig. 3f). In previous study [41], it was verified that the decomposition of PTFE leads to asymmetric evolution of the D and G bands. When an electrolyte with FEC was used, this relative symmetric evolution of the D and G bands occurs and exhibited higher I_D/I_G ratio (0.92). According to these analysis results, adding FEC in the electrolyte can alleviate the chemical deterioration of PTFE in the dry-processed anode, and that this change helps prevent battery performance degradation.

3.3. Post-mortem analysis about different binding properties of PTFE

To elucidate how the addition of FEC in the electrolyte affects the mechanical properties and degradation of the PTFE binder, which are crucial for preserving electrode integrity and performance, we carried out more intuitive characterizations (Fig. 4). Nanoindentation analysis was conducted to investigate the mechanical properties of the PTFE binder in local region of the dry-processed anodes in the different electrolytes (Fig. 4a). Detailed values of these mechanical properties can be found in Table S2. Notably, the dry-processed anode with FEC after 1 cycle exhibited a lower elastic modulus (17.80 MPa) compared to that without FEC (54.60 MPa). This lower stiffness of the dry-processed anode with FEC can be attributed to the suppressed decomposition of PTFE, which can lead to high elastic recovery against the volume change of graphite during cycling. The surface and interfacial cutting analysis system (SAICAS) was performed at the middle depth of each dry-processed anode to investigate the adhesion strength between the PTFE binders and the active materials (Fig. 4b). After 1 cycle, the dry-processed anode without FEC had lower adhesion strength (0.223 kN m^{-1}) than that of the anode with FEC (0.272 kN m^{-1}). This result suggests that an effective binding network system could not be maintained in the dry-processed anode without FEC because there is not enough protection for the PTFE binder. To assess the degradation of electrode due to the loss of binder properties, cross-sectional scanning electron microscopy (SEM) images were presented in Fig. 4(c–d). The dry-processed anode with FEC showed lower electrode thickness after 1 cycle (Fig. 4d) than that of the anode without FEC (Fig. 4c), which is contributed to the excellent elastic behavior during delithiation with improved binding network between the graphite particles and the PTFE binder in the electrode. In addition, the magnified cross-sectional and top-view SEM images show the evident morphological degradation of the PTFE binder (Fig. 4e and f) after cycling. As shown in Fig. 4e, the PTFE binder in the dry-processed anode after cycling without FEC becomes thick compared to the pristine PTFE binder before cycling, which is presented in Fig. S9, whereas the PTFE binder in the dry-processed anode after cycling with FEC retains its own morphologies without thickening. The morphological changes in PTFE depending on the use of the FEC additive stem from the demonstrated suppression of PTFE decomposition by FEC as evidenced in the electrochemical properties (Fig. 2). Moreover, the top-view SEM images of the electrode after

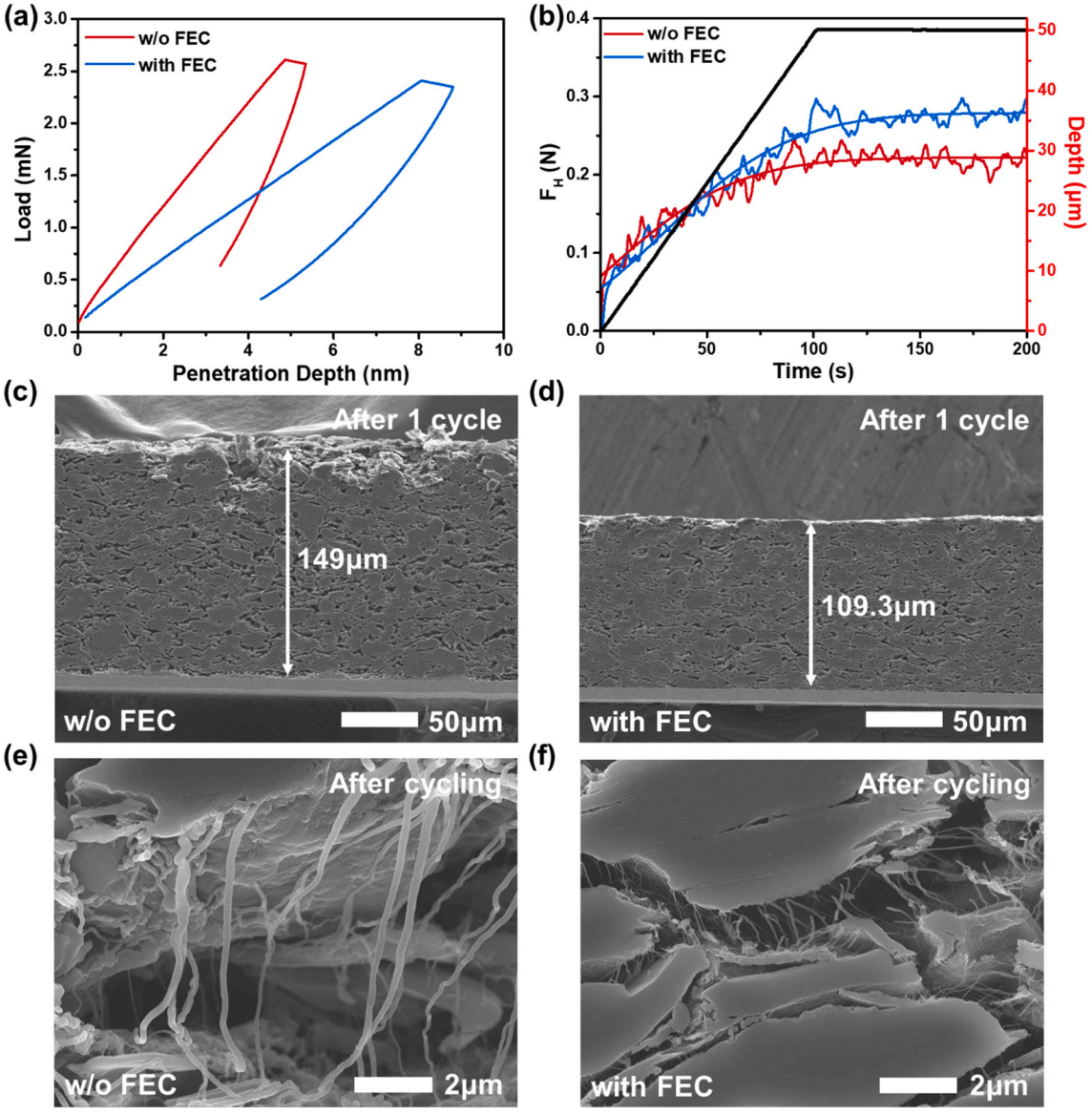

Fig. 4. Mechanical properties of dry-processed anode without and with FEC after 1 cycle. (a) The elasticity and (b) the adhesion strength of electrodes. The cross-sectional SEM images of dry-processed anode without and with FEC. (c–d) after 1 cycle and (e–f) after cycling.

cycling (Fig. S10) demonstrate that the degradation of PTFE after cycling without FEC leads to the widen distance between the graphite particles in the electrode, suggesting the deteriorated binding properties. Hence, the FEC additive effectively secured the binding properties of PTFE during cycling with reduced decomposition, and thereby aiding in the mitigation of electrode degradation following cycling.

3.4. Electrochemical performance of full cells

In order to demonstrate the improved electrochemical performance in the high-energy full cell by stabilization of PTFE with FEC additive, we fabricated coin-type full cells comprising the dry-processed anode and a lithium iron phosphate (LFP) cathode under high mass loading condition (Fig. 5). As shown in Fig. S11, while the full cell without FEC exhibited reversible capacity of 4.05 mAh cm^{-2} at the formation with the ICE of 72.5 %, the full cell with FEC demonstrated superior reversible capacity of 4.72 mAh cm^{-2} with the high ICE of 83.8 %. The voltage profile of the full cell without FEC clearly shows a sloping curve during charging process, indicating the PTFE decomposition reaction. The cycling performance of the full cells was evaluated at 1 mA cm^{-2} within the voltage range of 2.5–4.0 V. For the full cell with FEC, the stable cycling CE behaviors were retained during 100 cycles, and an outstanding capacity retention of 85.7 % after 100 cycles was achieved (Figs. 5a and S12). Similarly, to the improved cycle life in the half cell test, the cause of the superior cycle life of the full cell with FEC is regarded as the protection against PTFE decomposition which leads to great binding network throughout the thick electrode.

The Fig. 5b shows the rate capabilities of the full cells at diverse rates from 0.1 to 1.5C. For every third cycle at each C-rate, the full cell with FEC gave the discharge capacities of 130, 125, 121, 113, 90, and 53 mAh g^{-1} at 0.1, 0.2, 0.3, 0.5, 1.0, and 1.5C, respectively. On the contrary, the full cell without FEC delivered the discharge capacities of 96, 79, 71, 66, 40, and 25 mAh g^{-1} at 0.1, 0.2, 0.3, 0.5, 1.0, and 1.5C, respectively. This preeminent rate capabilities of the full cell with FEC were attributed to the excellent electrical pathway from the maintained binding property as well as the low resistances verified in Fig. 2f.

Additionally, we conducted further investigation into the efficacy of FEC in the dry-processed anode under ultra-high mass loading condition, with a target of 7.5 mAh cm^{-2} cathode areal capacity (8.25 mAh cm^{-2} anode areal capacity). Notably, while the slurry-processed anode suffered from significant cracking after the calendering process, the dry-processed anode was successfully fabricated without any cracks (Fig. S13). The cross-sectional SEM image in Fig. S14 shows the well-crafted electrode using dry electrode technology. The cycling performance of the full cell, which included this dry-processed anode and the LFP cathode with ultra-high mass loading was evaluated with and without FEC (Fig. 5c). Following the formation step, the full cell achieved a discharge capacity of 7.5 mAh cm^{-2} as indicated in Fig. S15. Remarkably, the ultra-high mass loaded full cell with FEC exhibited an average coulombic efficiency of 99.92 % during cycling and manifested excellent cyclability until 200 cycles.

A pouch full cell was also demonstrated to explore the potential for commercial battery applications (Fig. 6). The pouch cell was evaluated under the same test conditions as coin full cells. The pouch cell using electrolyte with FEC not only had reversible discharge capacity of 54.7 mAh but also exhibited the stable coulombic efficiency and cycling performances, showing possibility towards practical application. These outstanding electrochemical performances of the full cell, featuring the dry-processed anode with FEC under the high mass loading, suggests that the FEC additive plays a pivotal role in retarding PTFE decomposition and enhancing electrode stability while preserving the binding property.

4. Conclusion

In this work, we demonstrate the effect of the FEC additive as an interface stabilizer to alleviate the electrochemical instability of PTFE binder in dry-processed anode. This is the critical problem related to cost-effectiveness and high energy density in dry electrode technology, to the best of our knowledge, it has not been proved in dry-processed anodes. Here, the FEC-derived SEI formed on the surface of the electrode materials successfully diminished the irreversible reaction of PTFE and kept its mechanical properties. Consequently, the alleviated PTFE degradation under electrolyte with FEC indicate the considerable improvement of ICE (from 72.5 to 83.8 %) and capacity retention (from 53.7 to 85.7 % after 100 cycles) at areal capacity of 4.8 mAh cm^{-2}.

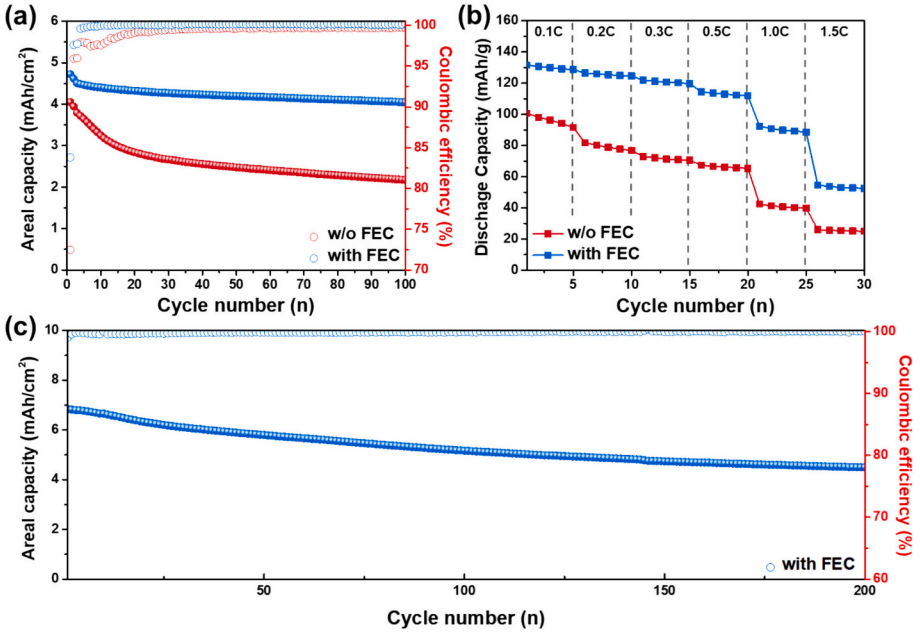

Fig. 5. Electrochemical performances of full cells under cathode areal capacity of 4.8 mAh cm^{-2} (anode areal capacity of 5.28 mAh cm^{-2}) without and with FEC. (a) Cycling performances for 100 cycles (b) Rate capabilities; Electrochemical performances of full cell with areal capacity of 7.5 mAh cm^{-2} with FEC. (c) Cycle performances for 200 cycles.

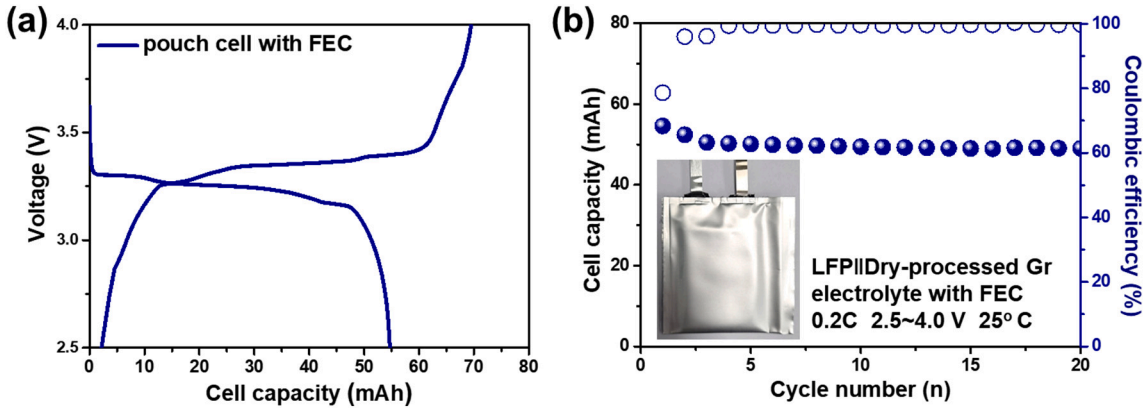

Fig. 6. Electrochemical performances of single layer pouch full cell using electrolyte with FEC. (a) voltage profile at 1st cycle (b) Cycle performances for 20 cycles.

Furthermore, the dry-processed anode under ultrahigh areal capacity (7.5 mAh cm^{-2}) exhibited excellent cycling stability for up to 200 cycles in a full cell with an LFP (as evidence by average CE of 99.92 % and stable capacity retention). Our design strategy for mitigating the irreversible reaction of PTFE in electrolyte with FEC would provide a special guideline for the progress of high-energy LIB in dry-processed anode system.

CRediT authorship contribution statement

Seungmin Han: Writing – review & editing, Writing – original draft, Investigation, Formal analysis, Data curation, Conceptualization. **Eui-Hyurk Noh:** Writing – original draft, Methodology, Investigation, Formal analysis, Data curation. **Sujong Chae:** Writing – review & editing, Writing – original draft, Visualization, Data curation, Conceptualization. **Kihwan Kwon:** Methodology, Data curation. **Juhyun Lee:** Methodology, Data curation. **Ji-Su Woo:** Methodology, Data curation. **Seongsu Park:** Methodology, Data curation. **Jung Woo Lee:** Methodology, Data curation. **Patrick Joohyun Kim:** Methodology, Data curation. **Taeseup Song:** Writing – review & editing, Supervision, Project administration, Conceptualization. **Won-Jin Kwak:** Writing – review & editing, Writing – original draft, Supervision, Project administration, Funding acquisition, Conceptualization. **Junghyun Choi:** Writing – review & editing, Writing – original draft, Visualization, Supervision, Project administration, Funding acquisition, Conceptualization.

Declaration of competing interest

The authors declare that they have no known competing financial interests or personal relationships that could have appeared to influence the work reported in this paper.

Data availability

Data will be made available on request.

Acknowledgements

This work was supported by the Industrial Strategic Technology Development Program (20024261, Development of thick film electrode and cell manufacturing technology for high-performance lithium iron phosphate battery with energy density of over 200 Wh/kg) and (20024252, Development of highly impregnative liquid electrolyte for high-performance lithium iron phosphate battery with thick electrode) funded by the Ministry of Trade, Industry & Energy (MOTIE, Korea).

Appendix A. Supplementary data

Supplementary data to this article can be found online at https://doi.org/10.1016/j.est.2024.112693.

References

[1] C.-W. Su, X. Yuan, R. Tao, M. Umar, Can new energy vehicles help to achieve carbon neutrality targets? J. Environ. Manag. 297 (2021) 113348.
[2] A. Al-Buenain, S. Al-Muhannadi, M. Falamarzi, A.A. Kutty, M. Kucukvar, N.C. Onat, The adoption of electric vehicles in Qatar can contribute to net carbon emission reduction but requires strong government incentives, Vehicles 3 (3) (2021) 618–635.
[3] J. Kim, G.R. Lee, R.B.K. Chung, P.J. Kim, J. Choi, Homogeneous Li deposition guided by ultra-thin lithiophilic layer for highly stable anode-free batteries, Energy Storage Mater. 61 (2023) 102899.
[4] J. Wen, D. Zhao, C. Zhang, An overview of electricity powered vehicles: lithium-ion battery energy storage density and energy conversion efficiency, Renew. Energy 162 (2020) 1629–1648.
[5] L. Lander, E. Kallitsis, A. Hales, J.S. Edge, A. Korre, G. Offer, Cost and carbon footprint reduction of electric vehicle lithium-ion batteries through efficient thermal management, Appl. Energy 289 (2021) 116737.
[6] J. Kwon, J. Kim, S.Y. Bae, S.P. Jeon, J.H. Song, S.E. Wang, D.S. Jung, J. Jang, H. Park, P.J. Kim, J. Choi, Polyanion-assisted ionic-electronic conductive agents designed for high density Si-based anodes, J. Power Sources 541 (2022) 231728.
[7] J. Kim, J. Choi, P.J. Kim, A new approach to stabilize the electrochemical performance of Li metal batteries through the structure alteration of CNT scaffolds, Carbon 203 (2023) 426–435.
[8] Y.-K. Sun, Promising all-solid-state batteries for future electric vehicles, ACS Energy Lett. 5 (10) (2020) 3221–3223.
[9] C.-Y. Wang, T. Liu, X.-G. Yang, S. Ge, N.V. Stanley, E.S. Rountree, Y. Leng, B. D. McCarthy, Fast charging of energy-dense lithium-ion batteries, Nature 611 (7936) (2022) 485–490.
[10] Y. Lu, C.-Z. Zhao, H. Yuan, J.-K. Hu, J.-Q. Huang, Q. Zhang, Dry electrode technology, the rising star in solid-state battery industrialization, Matter 5 (3) (2022) 876–898.
[11] J. Li, J. Fleetwood, W.B. Hawley, W. Kays, From materials to cell: state-of-the-art and prospective technologies for lithium-ion battery electrode processing, Chem. Rev. 122 (1) (2022) 903–956.
[12] G. Schälicke, I. Landwehr, A. Dinter, K.-H. Pettinger, W. Haselrieder, A. Kwade, Solvent-free manufacturing of electrodes for lithium-ion batteries via electrostatic coating, Energy Technol. 8 (2) (2020) 1900309.
[13] W.B. Hawley, J. Li, Electrode manufacturing for lithium-ion batteries—analysis of current and next generation processing, J. Energy Storage 25 (2019) 100862.
[14] M. Ryu, Y.-K. Hong, S.-Y. Lee, J.H. Park, Ultrahigh loading dry-process for solvent-free lithium-ion battery electrode fabrication, Nat. Commun. 14 (1) (2023) 1316.
[15] K. Kwon, J. Kim, S. Han, J. Lee, H. Lee, J. Kwon, J. Lee, J. Seo, P.J. Kim, T. Song, J. Choi, Low-resistance LiFePO4 thick film electrode processed with dry electrode technology for high-energy-density lithium-ion batteries, Small Sci. 4 (5) (2024) 2300302.
[16] Y.S. Zhang, N.E. Courtier, Z. Zhang, K. Liu, J.J. Bailey, A.M. Boyce, G. Richardson, P.R. Shearing, E. Kendrick, D.J.L. Brett, A review of lithium-ion battery electrode drying: mechanisms and metrology, Adv. Energy Mater. 12 (2) (2022) 2102233.
[17] J. Klemens, L. Schneider, E.C. Herbst, N. Bohn, M. Müller, W. Bauer, P. Scharfer, W. Schabel, Drying of NCM cathode electrodes with porous, nanostructured particles versus compact solid particles: comparative study of binder migration as a function of drying conditions, Energy Technol. 10 (4) (2022) 2100985.
[18] Y. Kuang, C. Chen, D. Kirsch, L. Hu, Thick electrode batteries: principles, opportunities, and challenges, Adv. Energy Mater. 9 (33) (2019) 1901457.
[19] W. Yao, M. Chouchane, W. Li, S. Bai, Z. Liu, L. Li, A.X. Chen, B. Sayahpour, R. Shimizu, G. Raghavendran, M.A. Schroeder, Y.-T. Chen, D.H.S. Tan,

B. Sreenarayanan, C.K. Waters, A. Sichler, B. Gould, D.J. Kountz, D.J. Lipomi, M. Zhang, Y.S. Meng, A 5 V-class cobalt-free battery cathode with high loading enabled by dry coating, Energy Environ. Sci. 16 (4) (2023) 1620–1630.
[20] R. Tao, B. Steinhoff, X.-G. Sun, K. Sardo, B. Skelly, H.M. Meyer, C. Sawicki, G. Polizos, X. Lyu, Z. Du, J. Yang, K. Hong, J. Li, High-throughput and high-performance lithium-ion batteries via dry processing, J. Chem. Eng. 471 (2023) 144300.
[21] Y. Zhang, X. Xia, K. Ma, G. Xia, M. Wu, Y.H. Cheung, H. Yu, B. Zou, X. Zhang, O. K. Farha, J.H. Xin, Functional textiles with smart properties: their fabrications and sustainable applications, Adv. Funct. Mater. 33 (33) (2023) 2301607.
[22] Y. Zhang, F. Huld, S. Lu, C. Jektvik, F. Lou, Z. Yu, Revisiting polytetrafluorethylene binder for solvent-free lithium-ion battery anode fabrication, Batteries 8 (6) (2022) 57.
[23] M. Zhang, N. Liang, D. Hao, Z. Chen, F. Zhang, J. Yin, Y. Yang, L.-S. Yang, Recent advances of SiOx-based anodes for sustainable lithium-ion batteries, Nano Res. Energy 2 (2023) e9120077.
[24] S.N. Bryntesen, A.H. Strømman, I. Tolstorebrov, P.R. Shearing, J.J. Lamb, O. Stokke Burheim, Opportunities for the state-of-the-art production of LIB electrodes—a review, Energies 14 (5) (2021) 1406.
[25] H. Kim, J.H. Lim, T. Lee, J. An, H. Kim, H. Song, H. Lee, J.W. Choi, J.H. Kang, Ozone-treated carbon nanotube as a conductive agent for dry-processed lithium-ion battery cathode, ACS Energy Lett. 8 (8) (2023) 3460–3466.
[26] Y. Zhang, S. Lu, Z. Wang, V. Volkov, F. Lou, Z. Yu, Recent technology development in solvent-free electrode fabrication for lithium-ion batteries, Renew. Sust. Energ. Rev. 183 (2023) 113515.
[27] M. Zhang, M. Chouchane, S.A. Shojaee, B. Winiarski, Z. Liu, L. Li, R. Pelapur, A. Shodiev, W. Yao, J.-M. Doux, S. Wang, Y. Li, C. Liu, H. Lemmens, A.A. Franco, Y. S. Meng, Coupling of multiscale imaging analysis and computational modeling for understanding thick cathode degradation mechanisms, Joule 7 (1) (2023) 201–220.
[28] Y. Li, Y. Wu, Z. Wang, J. Xu, T. Ma, L. Chen, H. Li, F. Wu, Progress in solvent-free dry-film technology for batteries and supercapacitors, Mater. Today 55 (2022) 92–109.
[29] G. Li, R. Xue, L. Chen, The influence of polytetrafluorethylene reduction on the capacity loss of the carbon anode for lithium ion batteries, Solid State Ionics 90 (1) (1996) 221–225.
[30] Q. Wu, J.P. Zheng, M. Hendrickson, E.J. Plichta, Dry process for fabricating low cost and high performance electrode for energy storage devices, MRS Adv. 4 (15) (2019) 857–863.
[31] M. Yoshio, R.J. Brodd, A. Kozawa, Lithium-Ion Batteries, Springer, 2009.
[32] S. Shiraishi, T. Kobayashi, A. Oya, Electrochemical lithium ion doping and undoping behavior of carbyne-like carbon film electrode, Chem. Lett. 34 (12) (2005) 1678–1679.
[33] Y. Zhang, S. Lu, F. Lou, Z. Yu, Leveraging synergies by combining polytetrafluorethylene with polyvinylidene fluoride for solvent-free graphite anode fabrication, Energy Technol. 10 (11) (2022) 2200732.
[34] S. Schweidler, L. de Biasi, A. Schiele, P. Hartmann, T. Brezesinski, J. Janek, Volume changes of graphite anodes revisited: a combined operando X-ray diffraction and in situ pressure analysis study, J. Phys. Chem. C 122 (16) (2018) 8829–8835.
[35] R. Petibon, C.P. Aiken, N.N. Sinha, J.C. Burns, H. Ye, C.M. VanElzen, G. Jain, S. Trussler, J.R. Dahn, Study of electrolyte additives using electrochemical impedance spectroscopy on symmetric cells, J. Electrochem. Soc. 160 (1) (2013) A117.
[36] C.H. Chen, J. Liu, K. Amine, Symmetric cell approach and impedance spectroscopy of high power lithium-ion batteries, J. Power Sources 96 (2) (2001) 321–328.
[37] X.-Q. Zhang, X.-B. Cheng, X. Chen, C. Yan, Q. Zhang, Fluoroethylene carbonate additives to render uniform Li deposits in lithium metal batteries, Adv. Funct. Mater. 27 (10) (2017) 1605989.
[38] S. Sun, S. Myung, G. Kim, D. Lee, H. Son, M. Jang, E. Park, B. Son, Y.-G. Jung, U. Paik, T. Song, Facile ex situ formation of a LiF–polymer composite layer as an artificial SEI layer on Li metal by simple roll-press processing for carbonate electrolyte-based Li metal batteries, J. Mater. Chem. A 8 (33) (2020) 17229–17237.
[39] T. Hou, G. Yang, N.N. Rajput, J. Self, S.-W. Park, J. Nanda, K.A. Persson, The influence of FEC on the solvation structure and reduction reaction of LiPF6/EC electrolytes and its implication for solid electrolyte interphase formation, Nano Energy 64 (2019) 103881.
[40] Y. Liu, Y. Huang, X. Xu, Y. Liu, J. Yang, J. Lai, J. Shi, S. Wang, W. Fan, Y.-P. Cai, Y.-Q. Lan, Q. Zheng, Fluorinated solvent-coupled anion-derived interphase to stabilize silicon microparticle anodes for high-energy-density batteries, Adv. Funct. Mater. 33 (40) (2023) 2303667.
[41] D.J. Lee, J. Jang, J.-P. Lee, J. Wu, Y.-T. Chen, J. Holoubek, K. Yu, S.-Y. Ham, Y. Jeon, T.-H. Kim, J.B. Lee, M.-S. Song, Y.S. Meng, Z. Chen, Physio-electrochemically durable dry-processed solid-state electrolyte films for all-solid-state batteries, Adv. Funct. Mater. 33 (28) (2023) 2301341.